Arabian Journal of Chemistry (2020) 13, 3963–3973

King Saud University

Arabian Journal of Chemistry

www.ksu.edu.sa
www.sciencedirect.com

ORIGINAL ARTICLE

Preparation and characterization of palladium/polypyrrole-reduced graphene oxide/foamed nickel composite electrode and its electrochemical dechlorination of triclosan

Zhaohui Zhang [a], Junjing Li [a,*], Cong Luan [a], Huan Wang [a], Xiuwen Cheng [b], Leqi Fang [a], Liang Wang [a,*], Bin Zhao [a], Chang Ma [a], Hongwei Zhang [a], Chunyan Li [c], Jinming Xu [d]

[a] *School of Environmental Science and Engineering, Tianjin Polytechnic University, State Key Laboratory of Separation Membranes and Membrane Processes, Binshui West Road 399, Xiqing District, Tianjin 300387, PR China*
[b] *Key Laboratory of Western China's Environmental Systems (Ministry of Education), Key Laboratory for Environmental Pollution Prediction and Control, Gansu Province, College of Earth and Environmental Sciences, Lanzhou University, Lanzhou 730000, PR China*
[c] *Tianjin Tianhaoyuan Technology Company Limited, Room 302, 13th Floor, Xiaoyuan New Village, Kaifa District, Tianjin 300457, PR China*
[d] *Tianjin Huayu Membrane Technology Co., Ltd., Room 209, 172 Huanghai Road, Tianjin 300457, PR China*

Received 7 January 2019; accepted 16 April 2019
Available online 26 April 2019

KEYWORDS

Pd/PPy-rGO/foam-Ni electrode;
Triclosan;
Electrocatalytic hydrodechlorination;
Potentiostatic electropolymerization;
Applied potential

Abstract In this study, a new composite electrode of palladium (Pd) nanoparticles dispersed on polypyrrole-reduced graphene oxide (PPy-rGO) loaded on foam-nickel was achieved by galvanostatic method. Characterization of structures, morphology and crystallinity of the synthesized materials were investigated by scanning electron microscopes (SEM), transmission electron microscope (TEM), X-ray photoelectron spectroscopy (XPS), X-ray diffraction (XRD), Raman spectroscopy and electrochemical impedance spectroscopy (EIS). The results of XPS and XRD demonstrated Pd showed primarily as Pd0. From SEM and TEM results, we had seen that Pd nanoparticles were dispersible well on the composite electrode. Raman spectroscopy was used to show the state of graphene oxide and further demonstrated that PPy and rGO had existed of on the foam Ni matrix. The data of EIS also suggested the charge transfer of the new composite electrode decreased compared

* Corresponding authors.
E-mail addresses: junjingli85@163.com (J. Li), mashi7822@163.com (L. Wang).
Peer review under responsibility of King Saud University.

Production and hosting by Elsevier

https://doi.org/10.1016/j.arabjc.2019.04.006

to Pd/PPy/foam-Ni and PPy/foam-Ni composite electrodes. The effect of the electropolymerization potential on Pd/PPy-rGO/foam-Ni electrode for removing triclosan (TCS) was examined. It was found that the removal efficiency of TCS on the composite electrode could reach 100% at electropolymerization potential of 0.7 V and reaction time of 100 min.

1. Introduction

Pharmaceuticals and personal care products (PPCPs) have caused great concern in last several years, because they are harmful for ecosystems and human health, which include antibiotics, hormones, antimicrobial agents, sunscreen products etc. (Wang et al., 2018; Zhu et al., 2018) Triclosan (TCS) is a largely used antimicrobial compound and a typical PPCP pollutant in natural aquatic systems (Murugesan et al., 2011; Buth et al., 2010). The Chemical structure of TCS is similar to brominated diphenyl ethers. It was firstly used in a surgery formation as an antibacterial component in 1972. TCS was widely used in antiseptics; toothpaste, deodorantand even textiles (Yueh et al., 2014). After it entered human body, TCS was primarily detoxified through glucuronidation by UDP-glucuronyl transferases (Moss et al., 2000). Previous studies showed that TCS could interfere with several hormones as endocrine disrupting chemical in various species and impair muscle contraction (Devito, 2007; Cherednichenko et al., 2012). Recently, more and more researchers focus their attention on removing the chlorinated organic compounds of water through electrochemical dechlorination method (Tsyganok, 2006; Laine and Cheng, 2007). The technology of electrochemical reductive detoxification and dechlorination of chlorinated organic compounds (Cheng et al., 2004) is called electrocatalytic hydrodehalogenation (ECH). This technology is one of the most prospecting innovative technologies with many merits, for example, high efficiency, low apparatus expense, gentle reaction conditions, easy operations and lack of secondary pollutants (Ge et al., 2005; Cheng et al., 2004). In the ECH process, electrodes were of high importance. Pd possessed excellent efficiency in H* maintenance via adsorption of H* on the surface and absorbed H* into Pd crystal lattice, which will result in a good electrocatalytic hydrodechlorination. Depositing them on preformed substrates based on polymer film has been considered with an attractive prospect (Qu et al., 2010; Pandey and Lakshminarayanan, 2009; Nagashree and Ahmed, 2009; Lee et al., 2002; Chmielewski et al., 2010).

Morphology and dispersity of catalytic metals have a close contact with catalytic property of the whole electrode in electrode catalytic system. Nickel foam has desirable three-dimensional network structure, large specific surface area and good electrical conductivity. Therefore, it can be used as support for Pd catalysts. Conductive polymers are appropriate as carriers of catalytic metals because of their large specific surface area and steady structure (Yang et al., 2009). The introduction of conductive polymers can improve not only the active area of matrix changing load situations of metals, but also the dispersion of metal particles which can increase the materials' activation behaviors. Among other polymers, polypyrrole (PPy) was one of the most attractive materials due to its good conductivity and stability, high electronic conductivity and cheap price that is easy to obtain (Turhan et al., 2011; Wang et al., 2008; Cui et al., 2008). Many researchers discovered that catalytic electrode modified by PPy could significantly improve electrocatalytic performance of the oxidation of organic molecules, such as methanol and methanoic acid, and its specific surface area increased obviously (Yang et al., 2007; Gautam and Suresh, 2006; Sun et al., 2008; Tsakova, 2008). PPy provided excellent matrixs for dispersing noble metals and had been used in the area of sensors and catalysts.

In recent years, graphene materials have generated considerable interest for their significant electrical, mechanical, and thermal performances (Novoselov et al., 2004; Rafiee, 2011; Lin et al., 2010; Bunch et al., 2007). In order to product graphene-based materials, one of the most common and convenient methods is the reduction of graphene oxide (GO). Due to its substantial oxygen functional groups, GO could be easily exfoliated to provide well-distributed organic solutions and aqueous as the precursor of graphene-based materials (William and Offeman, 1958; Si and Samulski, 2008; Fan et al., 2010; Stankovich et al., 2007; Li et al., 2008; Williams et al., 2008). The polypyrrole-reduced graphene oxide (PPy-rGO) composite could combine the electrical characteristics of graphene and the mechanical properties of polymers. And it could also show improved morphology characteristic and catalytic carrier applications, as comparison with those of pure PPy or graphene. There are many preparation methods of polypyrrole and other copolymer, including chemical polymerization, electrochemical polymerization, photochemistry polymerization and plasma polymerization. Electrochemical polymerization is driven by electric potential, making pyrrole polymerize at substrate directly and forming conductive film of PPy. The method above has the advantages of convenient use and simple operation, and it can adjust the morphology and thickness of film by controlling polymeric conditions (Yang and Huang, 2013). In this study, we adopt the potentiostatic polymerization as the preparation method of polypyrrole. In the situ electropolymerization process of polypyrrole, rGO was hoped to dope in the polypyrrole chain.

In this work, we developed a new Pd/PPy-rGO/foam-Ni composite electrode to efficiently remove triclosan. Due to reductive graphene oxide with anionic character, good electrical conductivity and large amount of oxygen functional groups, we investigated to incorporate reductive graphene oxide into PPy on foam-Ni. The conductivity and surface area of the composite electrode were improved by PPy-rGO film, which could provide more deposition sites for Pd nanoparticles. So far as we all know, there have been no reports about the material of PPy-rGO as middle-tier polymerized on foam-Ni electrode for electrochemical reduction system. Therefore, in this paper, we investigated the specific methods and the best conditions for preparing Pd/PPy-rGO/foam-Ni

composite electrode. The effect of different polymerized potentials of PPy-rGO on the morphology of composite electrode and property of electrocatalysis was also studied.

2. Experimental

2.1. Chemicals and reagents

Our chemical reagents were all the analytical grade except methanol, which was of chromatographic pure grade. Most of our chemical reagents were purchased from Sinopharm Chemical Reagent Co., Ltd. Platinum (Pt) foil was got from Shanghai Nonferrous Metal Co., Ltd. Foam nickel, whose surface density was 420 ± 25 g m^{-2}, was provided by Changsha Liyuan Material Co. Nafion-117 was the model of our proton exchange membrane used in electrocatalytic dechlorination. (DuPont, USA).

2.2. Preparation

Foam nickel plate (30 mm × 20 mm × 1 mm) was used in preparation by acetone and 0.5 mol L^{-1} H_2SO_4 under ultrasound. Potentiostatic polymerization of pyrrole and graphene oxide was prepared with three-electrode cell, which had a Luggin capillary in it. Saturated calomel electrode (SCE) and Pt electrode (20 mm × 10 mm × 0.2 mm) were used as the reference electrode and counter electrode, respectively. And foam nickel was selected as working electrode. The electrochemical polymerization was typically performed at a certain applied potential in the solution of 1.0 g L^{-1} of GO, 0.05 mol L^{-1}-pyrrole and 0.2 mol L^{-1} p-toluenesulfonic acid (PTS). The deposition of Pd nanoparticles on the PPy-rGO film was achieved by galvanostatic method. $PdCl_2$ solutions containing 3 mmol L^{-1} NaCl and 1 mmol L^{-1} $PdCl_2$ were prepared as needed. And the optimal palladium electrodeposition conditions was the constant current of 7 mA, temperature of 40 °C for 120 min. The colorless of solution implied the complete electrodeposition. Based on the experimental process above, the preparation procedure of Pd/PPy-rGO/foam-Ni was shown in Scheme 1.

2.3. Characterization

The surface morphology of composite electrodes was characterized by scanning electron microscopy (SEM, Hitachi S4800, Japan). The distribution of particle size on electrode was carried out by the transmission electron microscopy (TEM, Hitachi H7650, Japan). X-ray photoelectron spectroscopy (XPS) studies were carried out on D8 DISCOVER, Bruker. In Raman experiments, a multichannel Horiba XploRA plus spectrometer (λ = 532 nm) made in France was used. X-ray diffraction (XRD, Thermo fisher K-alpha, USA) is an effective way to analysis the crystalline structure of the electrode, which were recorded on Al Kα X-ray radiation. The binding energies (BE) were 284.6 eV, which was referenced with adventitious carbon. The electrochemical test of electrochemical impedance spectroscopy (EIS) was performed in Na_2SO_4 solution of 0.05 mol L^{-1} by Potentiostat (CHI660e) connected to a computer, and the frequency of measurements was between 10 mHz and 100 kHz. The ZSimpWin V3.10 was used to further analyze impedance spectra.

2.4. Electrocatalytic hydrodechlorination

The hydrodechlorination experiment was conducted with an H-shaped electrolyzer. The Pd/PPy-rGO/Ni composite electrode and platinum foil were used as cathode and anode, respectively. The volume of the catholyte and the anolyte were

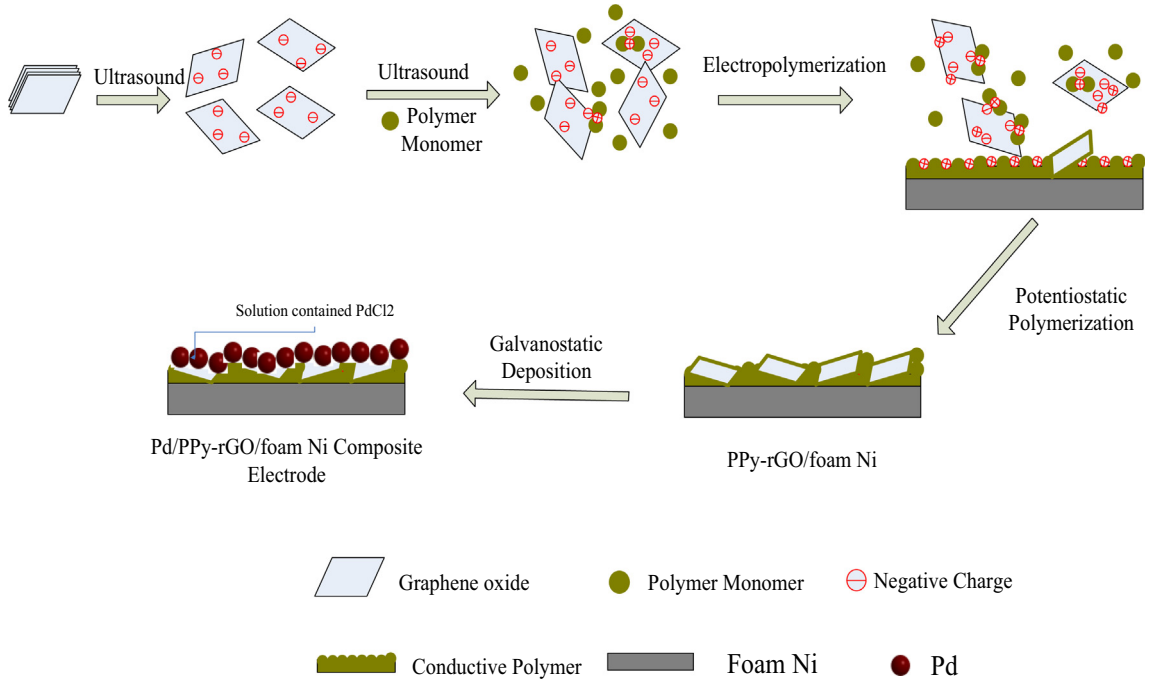

Scheme 1 The preparation procedure of Pd/PPy-rGO/Ni.

both 50 ml. The catholyte contained TCS of 50 mg L^{-1} and 0.05 mol L^{-1} Na_2SO_4 and the anolyte was 0.05 mol L^{-1} Na_2SO_4. The conditions of dechlorination experiments were 7 mA under the temperature of 40 °C. The LC-20A High-Performance Liquid Chromatograph (Shimadzu, Japan) and a UV detector (λ = 282 nm) were used to measure the concentration of TCS and dechlorinated products. An Inert Sustain C18 column was used (4.6 mm × 250 mm × 5 μm). The dissolved gas was removed by mobile phase by sonicating for 30 min before analysis.

3. Results and discussion

3.1. Morphology characterization of PPy-rGO film

The morphologies of PPy-rGO are imaged by SEM, as shown in Fig. 1 at different magnifications. As shown in 1a, the PPy-rGO film was uniformly dispersed on the foam Ni electrode. Under high magnification, the clustered PPy was grown at the surface of layered rGO, which was because of the strong interplay including hydrogen bonding, π-π stacking physical forces and van der Waals force between rGO and PPy.

The TEM images of PPy-rGO show common layered structure of rGO (Fig. 2). Fig. 2(a) and (b) depicted the uniformly-dense distribution of the PPy for the rGO layers, and the PPy almost evenly grow on the surface of rGO. The rGO is negatively charged, the polypyrrole is positively charged, and there are interactions between electrostatic attraction and π-π bond accumulation between the two materials (Zhu et al., 2012). The PPy, which exist between the layers of rGO, could prevent their aggregation of rGO.

3.2. Characterization of the Pd/PPy-rGO/Ni electrode

3.2.1. SEM, TEM and XPS spectra

SEM images examined the morphologies of Pd/PPy-rGO/foam-Ni composite electrode, as shown in Fig. 3. Under low magnification, Pd nanoparticles and the PPy-rGO film were clearly dispersed on foam Ni surface. When magnified, the cluster structure of PPy and plate form of rGO can be seen from Fig. 3(c) and (d). The concavo-convex surface morphologies of the composite electrode could provide Pd nanoparticles more active sites. The SEM mapping of Pd/PPy-rGO/foam-Ni electrode was shown in Fig. 4. From this Figure, it can be seen that Pd element disperse evenly.

The TEM images of Pd/PPy-rGO electrodes were presented to examine Pd particles deposited on PPy-rGO matrix in Fig. 5. The SAED pattern of Pd/PPy-rGO, which was shown in the inset of Fig. 5(a), demonstrated the presence of Pd nanoparticles. From its corresponding diffraction patterns, the diffraction rings of palladium (1 1 1), (2 0 0), (2 2 0), and (3 1 1) planes can be clearly seen, indicating that Pd nanoparticles have been grown mature. From larger amplifications of micrographs in Fig. 5(b), Pd nanoparticles were seen well dispersed on the PPy-rGO with average diameters of 5 nm. The PPy on rGO surface acted as anchoring sites for Pd nanoparticles and they could restrict the migration of Pd nanoparticles. The smaller the Pd particles were, the larger the contact area with the contaminants was, which was more conducive to the removal of contaminants.

XPS tests were examined the elemental chemical component of the new Pd/PPy-rGO/Ni electrode. And C1s, Nls, Pd3d and XPS survey spectra of the composite electrode were

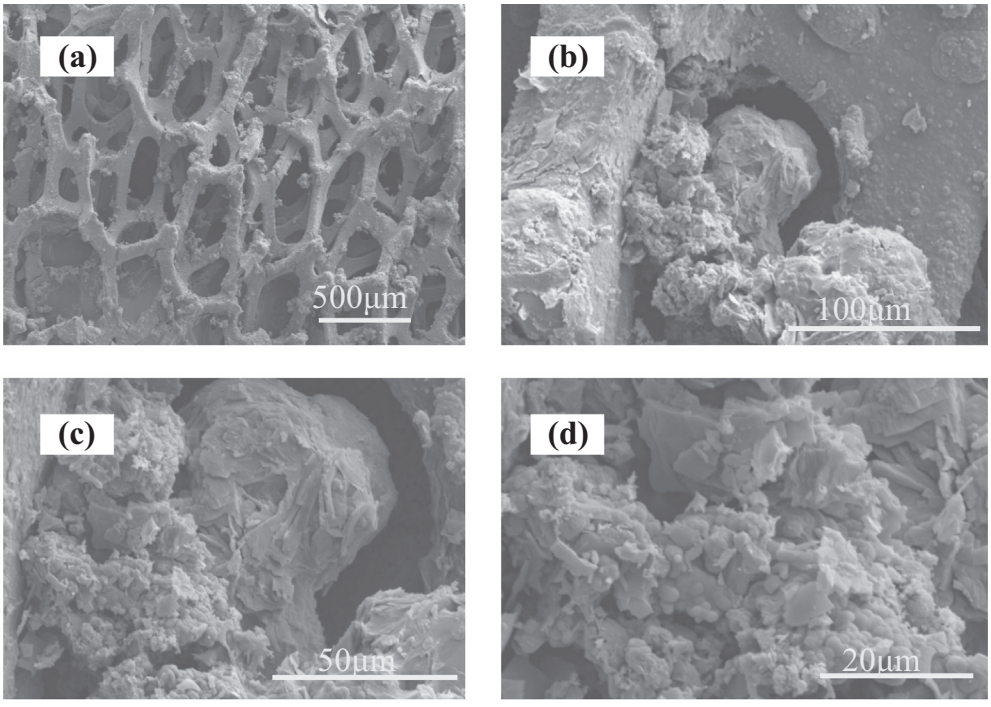

Fig. 1 SEM images of PPy-rGO/Ni electrodes at different magnifications (a) 50× (b) 500× (c) 1000× (d) 2000×.

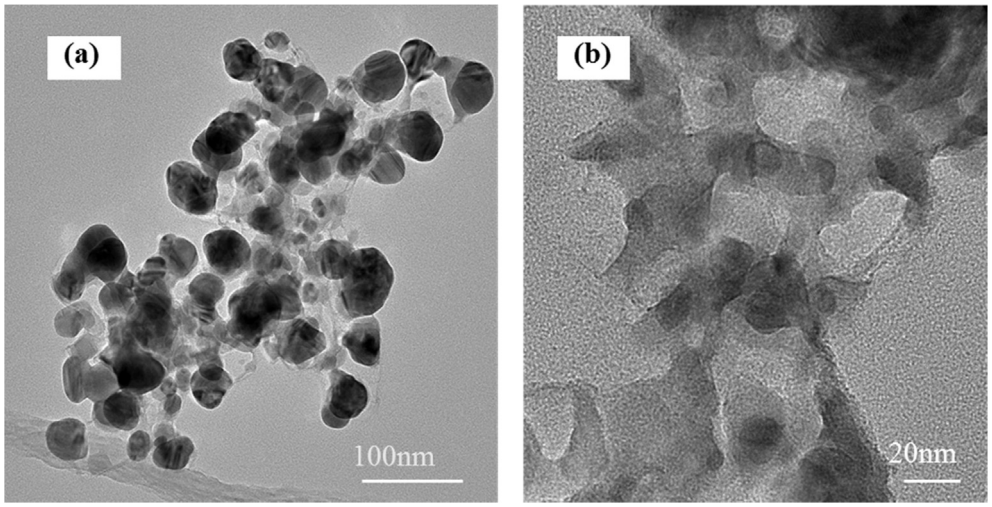

Fig. 2 TEM images of different magnification of PPy-rGO/Ni electrodes.

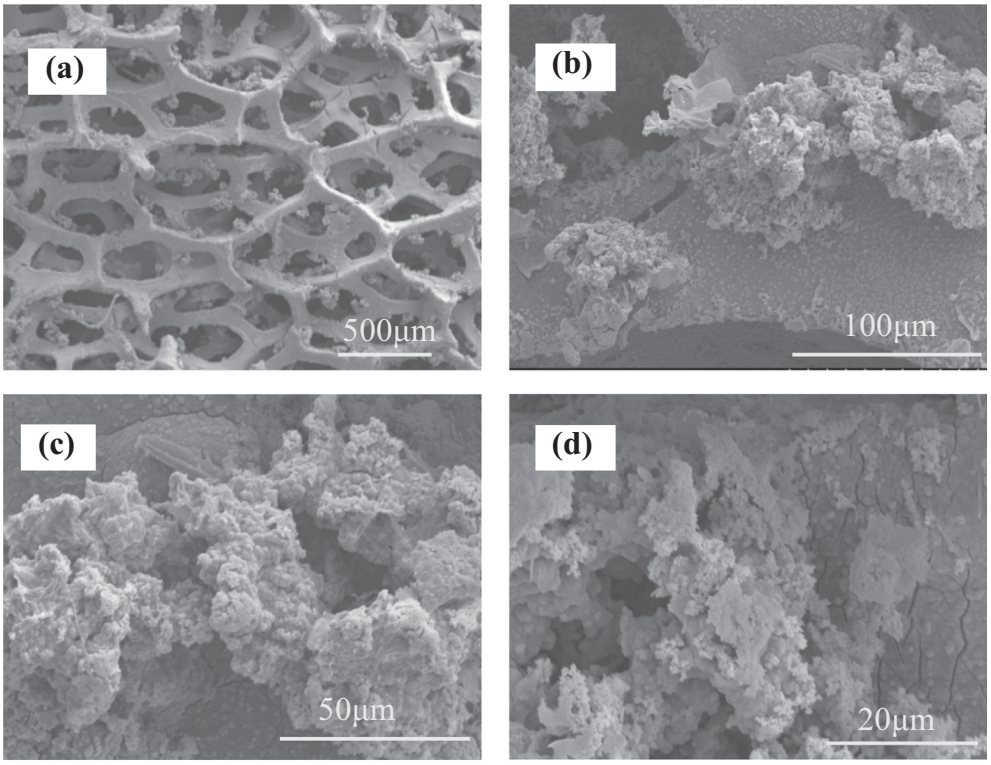

Fig. 3 SEM images of Pd/PPy-rGO/Ni electrodes at different magnifications (a) 50× (b) 500× (c) 1000× (d) 2000×.

shown in Fig. 6. Fig. 6(a) showed that the peaks centered at 284.5 and 288.5 eV were result in C—C/C—H and O—C=O (due to the over oxidation of PPy occurred at the β carbons of Py rings), respectively.

Moreover, the detected N originated from PPy. Fig. 6(b) showed the peak of nitrogen was broad, which indicated that there was more than one structures of nitrogen in the sample. Using peak separation software to make data fitting of nitrogen, we found that the peaks of 399.6 and 398.4 eV were corresponding to imine nitrogens (—NH—) and nitrate (—N=), respectively, and the peak of high bonding (401.1 eV) was corresponding to positive nitrogen ($—N^+$) (Dai et al., 2015). And the existence of $—N^+$ indicated PPy was present, that was to say that PPy was under oxidized state. As for PPy, the polaron of $—N^+$ was crucial to show its conductivity, because direct electrostatic interaction could facilitate conduction between the electron and positive charge (Zhu et al., 2012).

And Pd3d XPS image of Pd/PPy-rGO/Ni was shown in Fig. 6(c), which indicated that palladium had two states including Pd and Pd (II) whose Pd 3d3/2 and Pd 3d5/2 were at approximately 337.5 and 343 eV, 335.5 and 340.8 eV, respectively. The sample was mainly on metallic Pd though

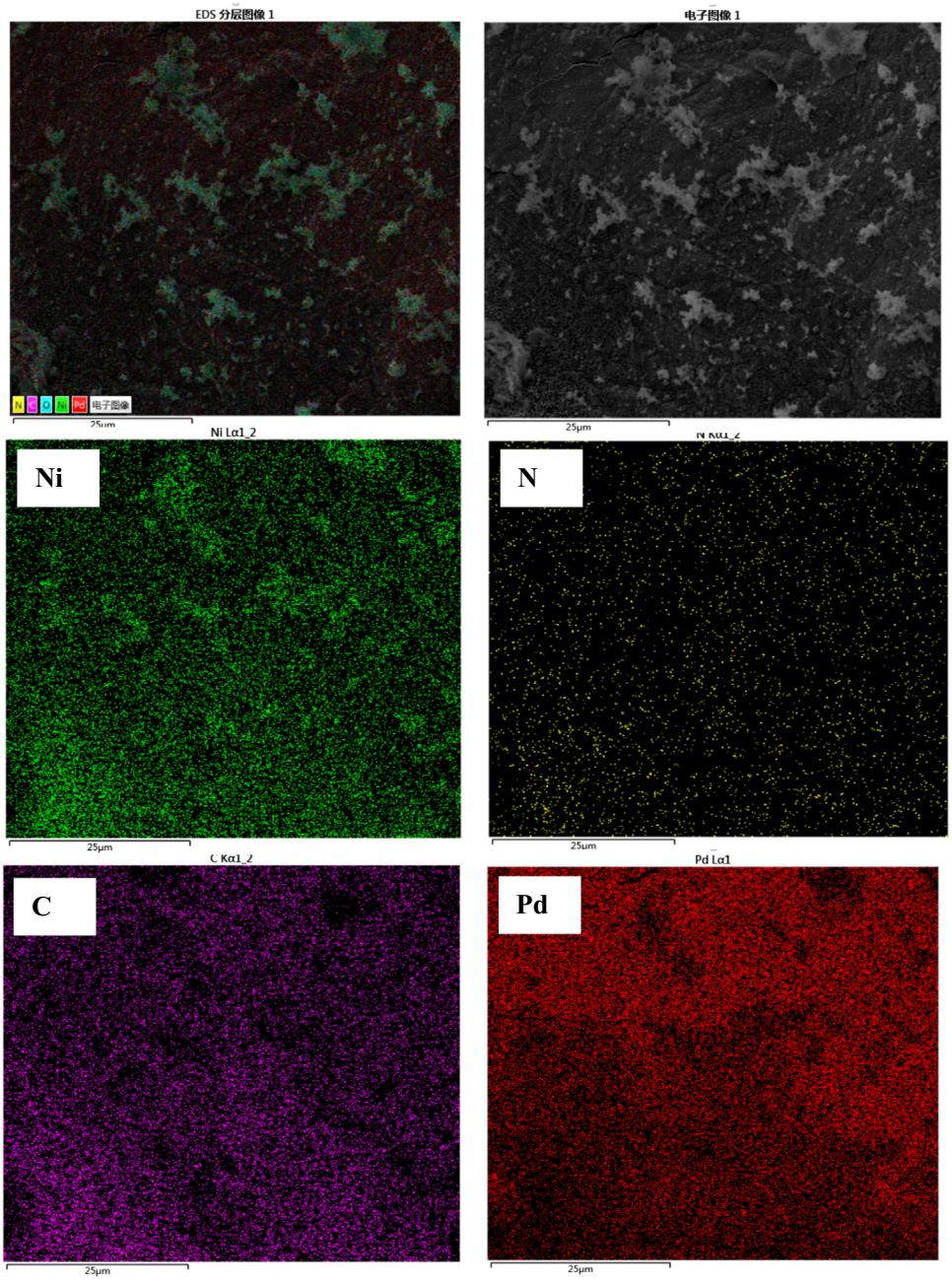

Fig. 4 SEM mapping of Pd/PPy-rGO/Ni electrode.

existing high state of Pd in it. Furthermore, in order to investigate the reduction degree of GO, C/O atomic ratio were showed in XPS measurement, which was one of the most direct techniques of analyzing reduction extent of GO and the carbon functionalities exist on graphene-based materials (Pruna et al., 2018). The XPS survey measurement was showed in Fig. 6(d), which displayed two peaks at about 530 and 284 eV which contributed to the O1s and C1s, respectively. It was observed that reduction extent decreased under various applied potentials: 0.7 V < 0.6 V < 0.8 V < 0.9 V, and the C/O ratios were 0.375, 0.432, 0.446 and 0.494, respectively. The obtained result showed that the GO was well reduced when the applied potential was 0.7 V, indicating the electrode had better conductivity and more excellent electrocatalytic activity for ECH of contaminants. The XPS measurement on PPy-rGO/Ni was also conducted, shown in Fig. S1.

3.2.2. X-ray diffraction

XRD measurements was studied to show the crystalline nature of Pd/PPy-rGO/foam Ni, which was showed in Fig. 7. The sharp peaks at $2\theta = 39.890°$, 46.530°, 67.350°, 86.200°and 81.850° were contributed to the (1 1 1), (2 0 0), (2 2 0), (2 2 2) and (3 1 1) diffractions of Pd, respectively. It also showed that Pd mainly existed as (1 1 1) lattice plane and further confirm

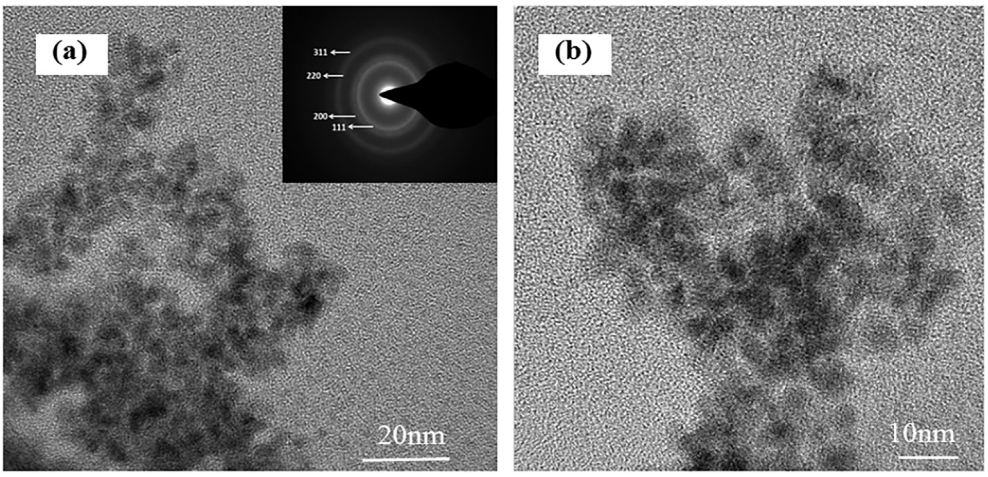

Fig. 5 SAED (a) and TEM images (b) of Pd/PPy-rGO /Ni electrodes.

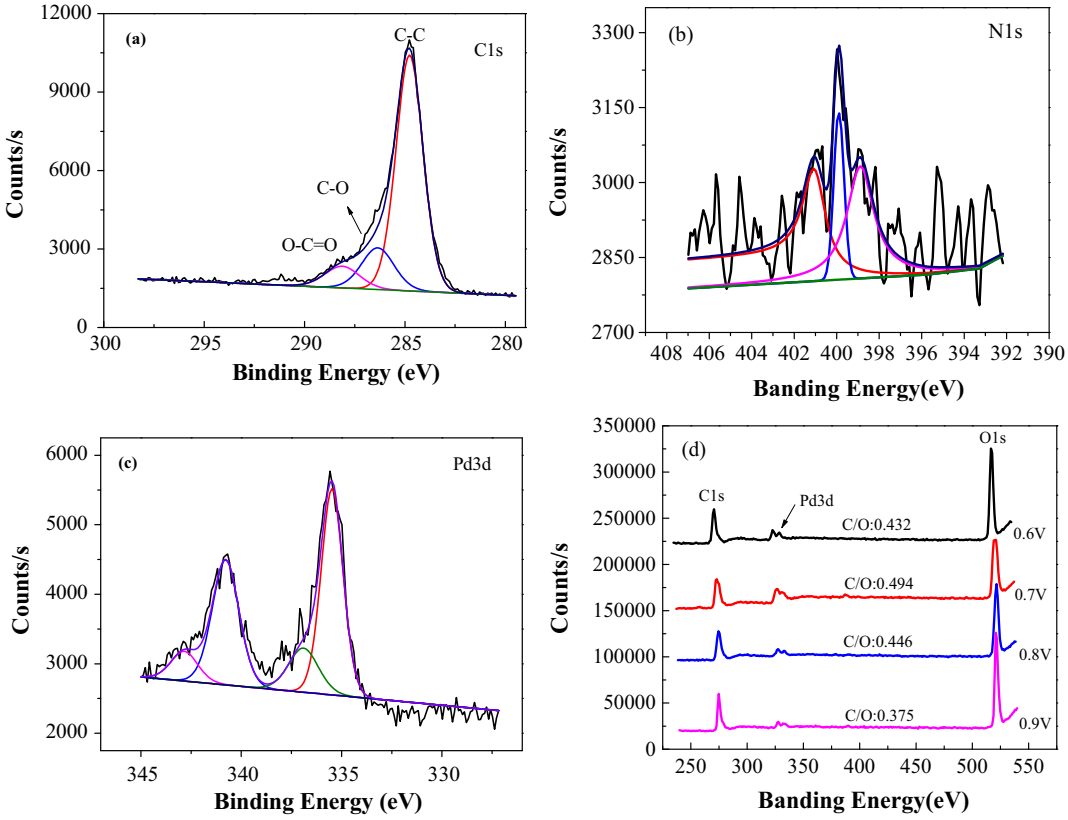

Fig. 6 C1s, Nls, Pd3d and XPS survey spectra of Pd/PPy-rGO/Ni composite electrodes.

that the presence of Pd nanoparticles in the prepared electrode. The $2\theta = 21.3°$ corresponds to the (0 0 2) crystal plane of carbon with an interplanar spacing of 0.76 nm of the rGO sheet due to the incorporation of oxygen functional groups between the basal planes of graphite, proving the existence of rGO in the material. According to the literature (Devi and Kumar, 2018) the (0 0 2) crystal plane of rGO at $2\theta = 10.1°$, the shift of the peak was due to the increasing intersheet caused by the intercalation of polymer between adjacent graphene oxide layers in the nanocomposites (Zhu et al., 2012).

3.2.3. Raman spectroscopy

Raman spectroscopy was used to further demonstrate the presence of PPy and rGO on the foam Ni surface (Fig. 8). The Raman spectrum of the PPy-rGO sample showed the existence of G and D bands at 1596 and 1348 cm^{-1}, of which G band represented the bond stretching of all pairs of sp^2 atoms in both rings and chains, while D band was corresponding to the disordered and imperfect graphite (Harpale et al., 2017). PPy-rGO/foam-Ni electrodes also exhibited characteristic

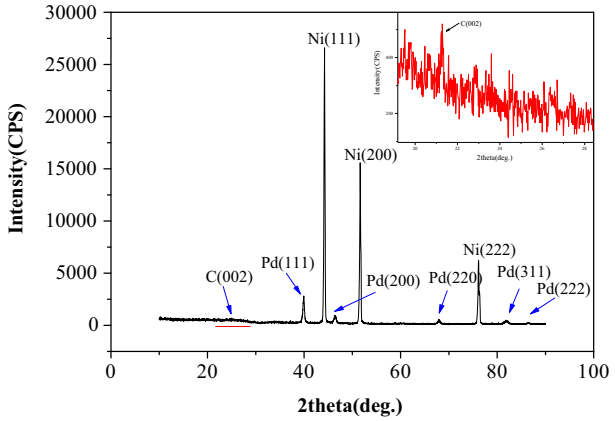

Fig. 7 XRD pattern of Pd/PPy-rGO/Ni electrode.

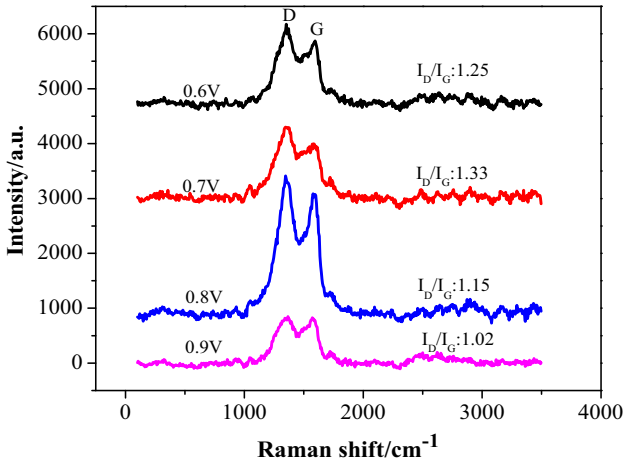

Fig. 8 Raman spectroscopy of Pd/PPy-rGO/Ni electrode under different applied potentials.

peaks of PPy and rGO. The D peak was higher than the G peak, which was caused by the growth orientation of graphene and indicated that the graphene defect was larger. The larger defects of graphene lead to the easier for electron conduction and the better cycle efficiency of the electrode.

In general, I_D/I_G, which represents the intensity ratio of the D band to G band, is studied to estimate the defect and degree of reduction among graphene materials. The higher ratio demonstrates the better reduction of GO and the increased amount of defects. The ratio of I_D/I_G at applied potential of 0.6, 0.7, 0.8 and 0.9 V were 1.25, 1.33, 1.15 and 1.02, respectively. So when the applied potential was 0.7 V, Pd/PPy-rGO/Ni displayed higher I_D/I_G ratio, suggesting the stronger reduction degree from GO, the larger surface area and active sites and the more beneficial to improvement of the electrocatalytic activity and electrochemical performance. The I_D/I_G ratio of rGO on PPy-rGO/Ni was also studied, shown in Fig S2. The I_D/I_G ratio was 0.799. Besides, the Tuinstra-Koenig (TK) relation ($La = (2.4 \times 10^{-10}) \times \lambda^4 \times (ID/IG)^{-1}nm$) was also studied to estimate the crystalline domain size (La) of composite electrodes which also depended on I_D/I_G ratio (Qiu et al., 2018). The La values of the prepared electrodes under applied potential of 0.6 V, 0.7 V, 0.8 V and 0.9 V were 15.38 nm, 14.45 nm, 16.71 nm and 18.85 nm, respectively. This indicated that the electrode under the applied potential of 0.7 V caused more reduction and defects of electrode materials.

3.2.4. Electrochemical impedance spectroscopy

In order to figure out the resistance data of the new electrode, electrochemical impedance spectroscopy analysis (EIS) has been investigated. The EIS spectra was studied to indicate the resistivity performances such as charge transfer resistance (Rct) and diffusion controlled process of the electrodes from 100 kHz to 10 mHz, as depicted in Fig. 9. To calculate the impedance parameters, the ZSimpWin software was used to simulate circuit model and diagram. The R(Q(R(Q(R(CR))))) is used as equivalent circuit to employ the impedance behavior of the following electrodes. Nyquist plot of impedance spectrum was formed form the linear portion at lower frequencies and the semicircle part at higher frequencies, correlating to the dispersal and the electron transfer process, respectively (Nia et al., 2015). Thus Pd/PPy-rGO/foam-Ni electrode exhibited the smallest semicircle at high frequencies, which indicated that the new electrode had the lowest Rct among these electrodes.

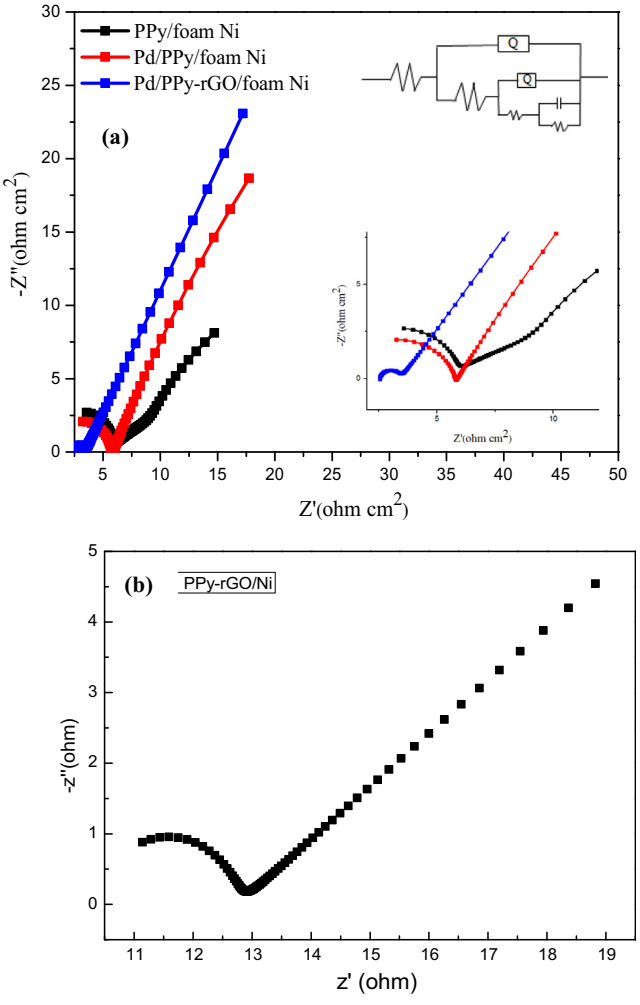

Fig. 9 Nyquist plot for PPy/foam-Ni, Pd/PPy/foam-Ni, Pd/PPy-rGO/foam-Ni electrodes (a) and Nyquist plot for PPy-rGO/Ni (b).

The predicted Rct values from Nyquist plot were 1.1 Ω, 4.8 Ω, 6.2 Ω for Pd/PPy-rGO/foam-Ni, Pd/PPy/foam-Ni, PPy/foam-Ni electrodes, respectively. Compared to the first two electrodes, the Rct value for the third was lower due to surface modification of electrodes, indicating the electrode was supposed to attributable for porous structure of rGO. Moreover, the porous structure of the new prepared electrode enabled the easier access to electrons, causing lower resistance in electrodes.

The calculated Nyquist plot slope value is commonly parallel to the imaginary axis, which shows that the electrode had a low ionic diffusion resistance and real capacitance behavior within the structure (Liu et al., 2013). The slope of Nyquist plot for different electrodes were Pd/PPy-rGO/foam-Ni > Pd/PPy/foam-Ni > PPy/foam-Ni, indicating that the modified electrode had lower diffusive resistance behavior of the electrolyte and better capacitive quality.

3.3. Effect of the applied potential of PPy-rGO

The polymerized potential has significant effect on the PPy-rGO film in the potentiostatic procedure. We examined the impact on the polymerized potential of PPy-rGO for electrochemical dechlorination of TCS of Pd/PPy-rGO/Ni electrode. Fig. 10 indicated that under polymerized potentials of PPy-rGO at 0.6, 0.7, 0.8, 0.9 V, the removal rates of TCS at 100 min were 96.37%, 100%, 93.82%, 96.82%, respectively. The result showed that when the applied potential was 0.7 V, the composite electrode reached the best removal efficiency. At higher applied potentials, the polymer had a faster growth rate, however, its conductivity became weaken (Harima et al., 2015). As the potentials descended, short polymer chains were easily formed and high redox states got easier for the electropolymerization procedure. Previous studies found that polymers with short chains had excellent conductivity because the local ordering of oligomers had increased (Bufon et al., 2010). Therefore, the optimum applied polymerization potential is 0.7 V.

Furthermore, the mathematical fitting of the remove of TCS under various applied potentials was studied on Fig. 9. The achieved results indicated that the electrochemical dechlorination reactions all followed the pseudo-first order reaction kinetics. The reaction kinetics constants of TCS at applied potential of 0.6 V, 0.7 V, 0.8 V and 0.9 V were 0.02836 min^{-1}, 0.04229 min^{-1}, 0.02948 min^{-1}, 0.01345 min^{-1}, which was in accord with the result of electrocatalytic dechlorination.

3.4. Stability

In order to investigate the cyclic stability of catalysts in practice applications, we had tested the stability of Pd/PPy-rGO/foam-Ni electrode. 5 times tests were experimentalized for removing of TCS to explore the stability of the prepared electrode. As shown in Fig. 11, the removal efficiency could still reach 93.05% after using for 5 times. The reaction products attached on the new electrode surface and the increase of adsorbate along with the reducing of active sites of Pd nanoparticles on the surface may led to the fall of the removal rate for 5 uses. Generally speaking, our new prepared electrode has great stability for practical applications. Thus, the recycle utilization for treating wastewater containing TCS of the new electrode was available and promising.

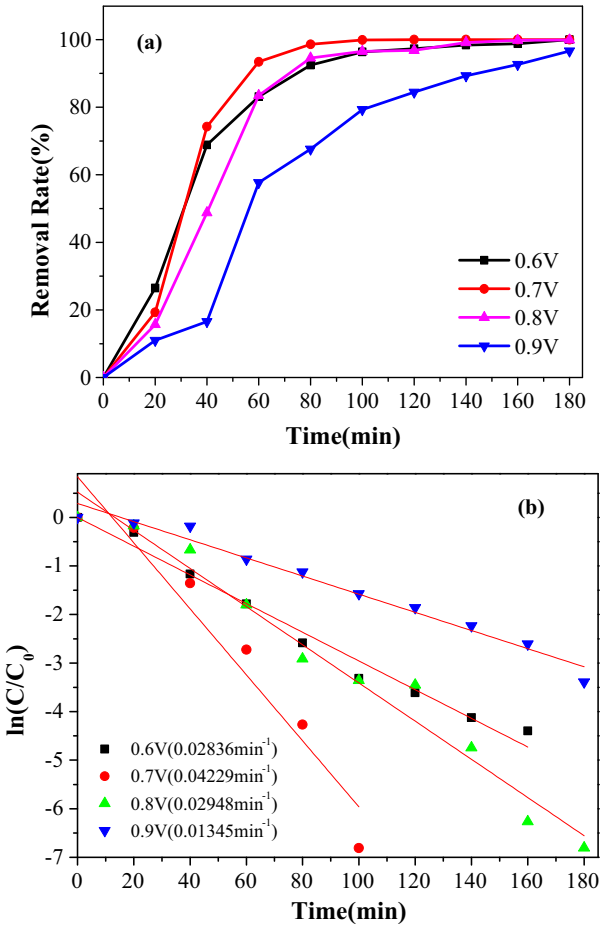

Fig. 10 The removal rate and kinetics of the ECH of TCS under different applied potential, (a) removal rate of TCS; (b) Kinetics of the ECH of TCS.

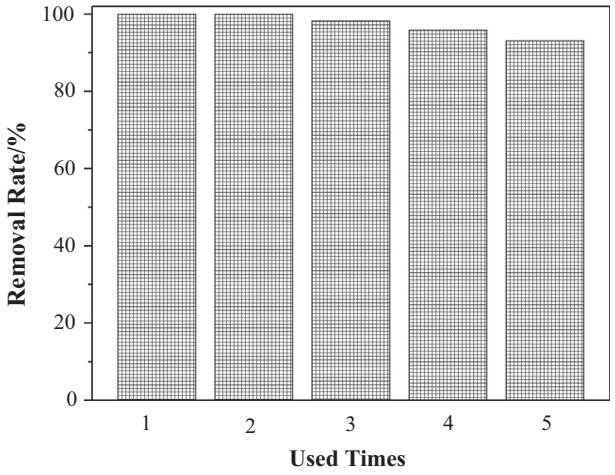

Fig. 11 Effect of repeat use of Pd/ PPy-rGO/ Ni on the removal of TCS.

4. Conclusion

In conclusion, we had successfully prepared the new Pd/PPy-rGO/foam-Ni electrode for electrochemical reduction of triclosan. PPy-rGO film was electrochemical polymerized on foam-Ni substrate by potentiostatic method. The best preparation conditions of PPy-rGO film for the new electrode were 0 °C under 20 min and a polymerized potential of 0.7 V in the solution with PTS. After, Pd particles were electrodeposited on the outermost layer of the new electrode under a constant current. Under this optimal condition, the removal rate of TCS reached 100% at 100 min. From XRD and XPS images, we obtained Pd mainly existed as Pd^0. The SEM and TEM investigated Pd particles were dispersed homogeneously. And different potentials effected on the electrode properties and electrochemical performance was studied. The prepared electrode showed significant electrochemical activity and stability, which might be attributed to the PPy-rGO film providing more active surface area and catalytic sites for Pd nanoparticles. All the results indicated the new prepared electrode has great prospect for electrochemical dechlorination applications.

Acknowledgments

This work was kindly supported by Natural Science Foundation of Tianjin of China (17JCQNJC07900), China Postdoctoral Science Foundation (2018M641656), National Natural Science Foundation of China (51508385, 51502201, 51508254, 51678408, 51638011), Scientific Research Plan Project of Tianjin Municipal Education Commission (2017KJ077), National Key R&D Program of China (Grant No. 2016YFE0106500), Tianjin Municipal Education Commission Research plan Projects (TJPU2k20170112), Fundamental Research Funds for the Central Universities (lzujbky-2015-137), the Science and Technology Plans of Tianjin (17PTSYJC00050), the National Key R&D Program of China (2016YFC0400506).

Appendix A. Supplementary material

Supplementary data to this article can be found online at https://doi.org/10.1016/j.arabjc.2019.04.006.

References

Bufon, C.C.B., Heinzel, T., Espindola, P., Heinze, J., 2010. Influence of the polymerization potential on the transport properties of polypyrrole films. J. Phys. Chem. B 114, 714–718.

Bunch, J.S., Zande, A.M., Verbridge, S.S., Frank, I.W., Tanenbaum, D.M., Parpia, J.M., Craighead, H.G., McEuen, P.L., 2007. Electromechanical resonators from graphene sheets. Science 315, 490–493.

Buth, J.M., Grandbois, M., Vikesland, P.J., Mcneill, K., Arnold, W. A., 2010. Aquatic photochemistry of chlorinated triclosan derivatives: Potential source of polychlorodibenzo-P-dioxins. Environ. Toxicol. Chem. 28, 2555–2563.

Cheng, H., Scott, K., Christensen, P.A., 2004. Design and operation of a solid polymer electrolyte reactor for electrochemical hydrodehalogenation. Chem. Eng. J. 102, 161–170.

Cheng, H., Scott, K., Christensen, P.A., 2004. Electrochemical hydrodehalogenation of 2,4-dichlorophenol in paraffin oil and comparison with aqueous systems. J. Electroanal. Chem. 566, 131–138.

Cherednichenko, G., Zhang, R., Bannister, R.A., Timofeyev, V., Li, N., Fritsch, E.B., Feng, W., Barrientos, G.C., Schebb, N.H., Hammock, B.D., 2012. Triclosan impairs excitation-contraction coupling and Ca^{2+} dynamics in striated muscle. Proc. Natl. Acad. Sci. USA 109, 16393. 16393-16393.

Chmielewski, M., Grzeszczuk, M., Kalenik, J., Kępas-Suwara, A., 2010. Evaluation of the potential dependence of 2D–3D growth rates and structures of polypyrrole films in aqueous solutions of hexafluorates. J. Electroanal. Chem. 647, 169–180.

Cui, C., Xie, Q., Yu, H., Han, Y., 2008. Electrocatalytic hydrodehalogenation of pentachlorophenol at palladized multiwalled carbon nanotubes electrode. Appl. Catal. B 80, 122–128.

Dai, T.Y., Wang, H.J., Cao, Y., Lu, Y., 2015. Preparation, characterization and application of polyaniline/epoxide polysiloxane composite films. Chin. J. Polym. Sci. 33, 732–742.

Devi, M., Kumar, A., 2018. 85 MeV C 6+ swift heavy ion irradiation of in-situ reduced graphene oxide–polypyrrole nanotubes nanocomposite films for supercapacitor electrodes. Electrochim. Acta 261, 1–13.

Devito, M.J., 2007. Short-term in vivo exposure to the water contaminant triclosan: Evidence for disruption of thyroxine. Environ. Toxicol. Pharmacol. 24, 194–197.

Fan, X., Peng, W., Li, Y., Li, X., Wang, S., Zhang, G., Zhang, F., 2010. Deoxygenation of exfoliated graphite oxide under alkaline conditions: a green route to graphene preparation. Adv. Mater. 20, 4490–4493.

Gautam, S.K., Suresh, S., 2006. Dechlorination of DDT, DDD and DDE in soil (slurry) phase using magnesium/palladium system. J. Colloid Interface Sci. 304, 144–151.

Ge, C., Wang, Z., Xia, D., 2005. Electrochemically reductive dechlorination of micro amounts of 2,4,6-trichlorophenol in aqueous medium on molybdenum oxide containing supported palladium. Electrochim. Acta 50, 933–937.

Harima, Y., Fukumoto, S., Zhang, L., Jiang, X., Yano, J., Inumaru, K., Imae, I., 2015. Thermoelectric performances of graphene/polyaniline composites prepared by one-step electrosynthesis. RSC Adv. 5, 86855–86860.

Harpale, K.V., Bansode, S.R., More, M.A., 2017. One-pot synthesis, characterization, and field emission investigations of composites of polypyrrole with graphene oxide, reduced graphene oxide, and graphene nanoribbons. J. Appl. Polym. Sci 134, 45170.

Laine, D.F., Cheng, I.F., 2007. The destruction of organic pollutants under mild reaction conditions: A review. Microchem. J. 85, 183–193.

Lee, S., Sung, H., Han, S., Paik, W., 2002. Polypyrrole film formation by solution-surface electropolymerization: influence of solvents and doped anions. J. Phys. Chem. 98, 1250–1252.

Li, D., Müller, M.B., Gilje, S., Kaner, R.B., Wallace, G.G., 2008. Processable aqueous dispersions of graphene nanosheets. Nat. Nanotechnol. 3, 101–105.

Lin, Y.M., Dimitrakopoulos, C., Jenkins, K.A., Chiu, H.Y., Grill, A., Avouris, P., 2010. 100-GHz Transistors from wafer-scale epitaxial graphene. Science 327, 662. 662-662.

Liu, Y., Zhang, Y., Ma, G., Wang, Z., Liu, K., Liu, H., 2013. Ethylene glycol reduced graphene oxide/polypyrrole composite for supercapacitor. Electrochim. Acta 88, 519–525.

Moss, T., Howes, D., Williams, F.M., 2000. Percutaneous penetration and dermal metabolism of triclosan (2,4, 4'-trichloro-2'-hydroxydiphenyl ether). Food Chem. Toxicol. 38, 361–370.

Murugesan, K., Bokare, V., Jeon, J.R., Kim, E.J., Kim, J.H., Chang, Y.S., 2011. Effect of Fe-Pd bimetallic nanoparticles on Sphingomonas sp. PH-07 and a nano-bio hybrid process for triclosan degradation. Bioresour. Technol 102, 6019–6025.

Nagashree, K.L., Ahmed, M.F., 2009. Electrocatalytic oxidation of methanol on Cu modified polyaniline electrode in alkaline medium. J. Appl. Electrochem. 39, 403–410.

Nia, P.M., Meng, W.P., Lorestani, F., Mahmoudian, M.R., Alias, Y., 2015. Electrodeposition of copper oxide/polypyrrole/reduced graphene oxide as a nonenzymatic glucose biosensor. Sens. Actuat., B 209, 100–108.

Novoselov, K.S., Geim, A.K., Morozov, S.V., Jiang, D., Zhang, Y., Dubonos, S.V., Grigorieva, I.V., Firsov, A.A., 2004. Electric field effect in atomically thin carbon films. Science 306, 666–669.

Pandey, R.K., Lakshminarayanan, V., 2009. Electro-oxidation of formic acid, methanol, and ethanol on electrodeposited Pd-polyaniline nanofiber films in acidic and alkaline medium. J. Phys. Chem. C 113, 21596–21603.

Pruna, A., Wu, Z., Zapien, J.A., Li, Y.Y., Ruotolo, A., 2018. Enhanced photocatalytic performance of ZnO nanostructures by electrochemical hybridization with graphene oxide. Appl. Surf. Sci. 441, 936–944.

Qiu, X., Xiao, Z., Wang, L., Fan, L.Z., 2018. High rate integrated quasi-solid state supercapacitors based on nitrogen-enriched active carbon fiber/reduced graphene oxide nanocomposite. Carbon 130, 196–205.

Qu, B., Xu, Y.T., Lin, S.J., Zheng, Y.F., Dai, L.Z., 2010. Fabrication of Pt nanoparticles decorated PPy–MWNTs composites and their electrocatalytic activity for methanol oxidation. Synth. Met. 160, 732–742.

Rafiee, M.A., 2011. graphene-based composite materials. Dissert. Theses - Gradworks 442, 282–286.

Si, Y., Samulski, E.T., 2008. Synthesis of water soluble graphene. Nano Lett. 8, 1679.

Stankovich, S., Dikin, D.A., Piner, R.D., Kohlhaas, K.A., Kleinhammes, A., Jia, Y., Wu, Y., Nguyen, S.B.T., Ruoff, R.S., 2007. Synthesis of graphene-based nanosheets via chemical reduction of exfoliated graphite oxide. Carbon 45, 1558–1565.

Sun, Z.R., Li, B.H., Xiang, H., Shi, M., Hou, Q.N., Peng, Y.Z., 2008. Electrochemical dechlorination of chloroform in neutral aqueous solution on palladium/foam-nickel and palladium/polymeric pyrrole film/foam-nickel electrodes. J. Environ. Sci. 20, 268–272.

Tsakova, V., 2008. How to affect number, size, and location of metal particles deposited in conducting polymer layers. J. Solid State Electrochem. 12, 1421–1434.

Tsyganok, A.I., 2006. Selective removal of chlorine from chloroaromatic pollutants by electrocatalytic reduction over palladium-loaded carbon felt. Res. Chem. Intermed. 32, 357–372.

Turhan, M.C., Weiser, M., Jha, H., Virtanen, S., 2011. Optimization of electrochemical polymerization parameters of polypyrrole on Mg–Al alloy (AZ91D) electrodes and corrosion performance. Electrochim. Acta 56, 5347–5354.

Wang, H., Lee, J.K., Moursi, A., Lannutti, J.J., 2008. Electrochemical degradation of 2,4-dichlorophenol on a palladium modified gas-diffusion electrode. Electrochim. Acta 53, 6402–6409.

Wang, S., Poon, K., Cai, Z., 2018. Removal and metabolism of triclosan by three different microalgal species in aquatic environment. J. Hazard. Mater. 342, 643–650.

William, S.H., Offeman, R.E., 1958. Preparation of graphitic oxide. J. Am. Chem. Soc. 80, 1339. 1339–1339.

Williams, G., Seger, B., Kamat, P.V., 2008. TiO_2-graphene nanocomposites. UV-assisted photocatalytic reduction of graphene oxide. ACS Nano 2, 1487.

Yang, Q.H., Huang, T.Z., 2013. Study of the preparation and property of oxygen reduction electrode based on polyaniline or polypyrrole. Appl. Mech. Mater 320, 639–643.

Yang, K.H., Liu, Y.C., Yu, C.C., 2009. Temperature effect of electrochemically roughened gold substrates on polymerization electrocatalysis of polypyrrole. Anal. Chim. Acta 631, 40–46.

Yang, B., Yu, G., Shuai, D., 2007. Electrocatalytic hydrodechlorination of 4-chlorobiphenyl in aqueous solution using palladized nickel foam cathode. Chemosphere 67, 1361–1367.

Yueh, M.F., Taniguchi, K., Chen, S., Evans, R.M., Hammock, B.D., Karin, M., Tukey, R.H., 2014. The commonly used antimicrobial additive triclosan is a liver tumor promoter. Proc. Natl. Acad. Sci. USA 111, 17200.

Zhu, L., Shao, Y., Xiao, H., Santiago-Schübel, B., Meyer-Alert, H., Schiwy, S., Yin, D., Hollert, H., Küppers, S., 2018. Electrochemical simulation of triclosan metabolism and toxicological evaluation. Sci. Total Environ. 622–623, 1193–1201.

Zhu, C.Z., Zhai, J.F., Wen, D., Dong, S.J., 2012. Graphene oxide/polypyrrole nanocomposites: one-step electrochemical doping, coating and synergistic effect for energy storage. J. Mater. Chem. 22, 6300–6306.